# Effect of slags of different origins and the role of sulfur in slag on the hydration characteristics of cement-slag systems

Zhang, Yu; Schlangen, Erik; Copuroglu, Oguzhan

**DOI**
10.1016/j.conbuildmat.2021.125266

**Publication date**
2022

**Document Version**
Final published version

**Published in**
Construction and Building Materials

Construction and Building Materials 316 (2022) 125266

Contents lists available at ScienceDirect

Construction and Building Materials

journal homepage: www.elsevier.com/locate/conbuildmat

# Effect of slags of different origins and the role of sulfur in slag on the hydration characteristics of cement-slag systems

Yu Zhang *, Erik Schlangen, Oğuzhan Çopuroğlu

*Microlab, Faculty of Civil Engineering and Geosciences, Delft University of Technology, Delft, The Netherlands*

ARTICLE INFO

*Keywords:*
Commercial and synthetic slag
Origin
Sulfur
$C_3S$-slag system

ABSTRACT

The effect of slag of different origins (synthetic slag produced in the laboratory and commercial slag collected from different steel factories) with comparable chemical composition, amorphous content and particle size distribution, on the hydration characteristics of slag cement was investigated. In order to study the effect of sulfur in slag, a model cement paste of a $C_3S$-slag blend was also produced. It was found that origin of slag has very little impact on the hydration process of cement-slag system. Synthetic slag shows a comparable compressive strength gain to commercial slag at 1 day, and from then on, a lower compressive strength is reached by it compared with that of commercial slag until 28 days. The sulfur in slag starts to participate in reaction after 1 day and it dominates the rate of heat release in calorimetric measurement, consistent with the result of compressive strength test. It significantly affects the elemental composition of the cementitious matrix at 7 days, and higher Al/Si and S/Ca ratios can be detected in cement-commercial slag blend at 7 days. The sulfur is involved in the formation of AFm-phase, such as calcium monosulfoaluminate, and the thermodynamic modelling shows that upon the gradual incorporation of sulfur in slag, calcium monosulfoaluminate precipitates continuously with the consumption of strätlingite and portlandite. The conclusion obtained in the paper provides a basis to understand the role of sulfur in slag on the hydration process of slag cement

## 1. Introduction

Blast furnace slag is a byproduct from pig iron production and it has been used as a mature addition in cement industry for several decades, especially in European and north American countries [1–4]. The chemical composition of slag varies depending on the origin significantly, such as where iron ore imported, fluxing stone and impurity of coke fed into the blast furnace [5]. Owing to its lower density, the molten slag forms on top of the molten iron liquid in the furnace, which is composed of lime, silica, alumina and magnesia, and could be identified as a $CaO–SiO_2–Al_2O_3–MgO$ system. When water-quenched rapidly, it shows vitreous structure with a latent hydraulic property which makes ground granulated slag a high-quality pozzolanic component in blended cement. However, because pig iron production has become a costly process due to increased consumption of iron ore across the world and the increasing cost of energy. As a result, low-grade raw materials have been fed into the furnace to reduce production cost, which according to [5–7], likely to have changed the chemical composition and pozzolanic properties of slag. Therefore, the different origins of slag has intensified the concern from industry on its quality/reactivity used as supplementary cementitious material in cement.

Recently, some studies [8–10] used synthetic glass, a $CaO–SiO_2–Al_2O_3$ system in principle, to investigate the effect of metal oxides on the reactivity of glass. It was demonstrated that chemical composition played a key role on the network structure of glass, which would affect reactivity. Obviously, the interaction between MgO and $CaO–SiO_2–Al_2O_3$ system was not taken into consideration in these studies, and their conclusions based on this system cannot be applied to a $CaO–SiO_2–Al_2O_3–MgO$ (slag) system directly. Furthermore, questions like whether synthetic glass produced in the laboratory behaves similar to commercial slag in a real cementitious environment has also been raised by the industry.

The sulfur (S) in slag comes from iron pyrite used as raw material and fuel for energy. It exists as anion $S^{2-}$ in the molten slag liquid. During quenching, it will emit in the form of $H_2S$ with water vapor. The $H_2S$ emission, dependent on the molten slag liquid and granulation water temperature as well as the slag/water ratio, will be precipitated in condensation tower finally. On the other hand, the rest which do not

* Corresponding author.
*E-mail addresses:* Y.Zhang-28@tudelft.nl (Y. Zhang), Erik.Schlangen@tudelft.nl (E. Schlangen), O.Copuroglu@tudelft.nl (O. Çopuroğlu).

https://doi.org/10.1016/j.conbuildmat.2021.125266
Received 18 August 2021; Received in revised form 20 September 2021; Accepted 12 October 2021
Available online 9 December 2021

emit exist as sulfide in slag, whereas it is presented in the form of $SO_3$ by XRF. European Standard EN 15167-1 requires that the sulfide and sulfate contents in slag should be ≤2.0% and 2.5% respectively. The main concern is the delayed formation of ettringite when exceeding this certain amount, which may impose a negative impact on the mechanical property of hardened slag cement. Also, doubts were being expressed that whether the sulfide content of slag would promote reinforcement corrosion. After 27 years of seawater storage, no related problems had occurred [11]. The presence of several sulfur anions, such as $S^{2-}$, $S_2O_3^{2-}$ and $SO_4^{2-}$, has been reported in leachates of hydrated cement containing slag [12–14]. Oxidation to the most stable product, i.e. $SO_4^{2-}$ can take weeks by molecular oxygen at pH > 8.5 considering the alkaline and mildly reductive environment occurring in the pore solution of slag cement [15]. Nonetheless, the role of sulfur in slag on the hydration evolution has been largely neglected, possibly because the introduction of $S^{2-}$ ion by slag does not appear to affect mechanical properties, thus it does not attract much attention from the researchers.

In the present research we will lay emphasis on the effect of slag of different origins with almost the same chemical composition and amorphous content, and the role of sulfur in slag on the hydration characteristics of slag cement. Three slags were employed here, one was produced in the laboratory with pure reagent and the other two were offered by Ecocem Benelux B.V. collected from different steel factories. To investigate the effect of slag of different origins, the paper analyzes the heat evolution of slag cement paste with isothermal calorimeter, the formation of calcium hydroxide and the content of bound water by means of thermogravimetric analysis, the development of microstructure by mercury intrusion porosimetry and back-scattered electron imaging of selected sample. To characterize the effect of sulfur from slag specifically, model paste specimen containing only $C_3S$ ($3CaO•SiO_2$) and slag was prepared additionally.

## 2. Material and methodology

### 2.1. Materials

CEM I 425N (manufactured by ENCI Maastricht BV), coarse-granulated commercial slag CS1 and fine-granulated commercial slag CS2 of different origins (provided by Ecocem Benelux BV) were used. The synthetic slag (SS) was produced to be incorporated in the cement-slag system. Model $C_3S$-slag system was employed to study the effect of sulfur in slag specifically. Quartz was also introduced to produce cement-quartz system and act as reference for comparison. The chemical composition and selected physical properties of the raw materials are presented in Table 1. The particle size distributions of three slags and quartz were measured by laser diffraction and is shown in Fig. 1.

Fig. 2 elaborates the XRD scan of slag, showing that they were entirely amorphous without a significant peak indicating crystallinity. Also, no positional shift of the amorphous hump was observed; fluctuating at around 30° (2θ).

### 2.2. Mix design and experimental method

All raw materials were in weight percentage (wt.%) with respect to the total binder content. To understand the effect of sulfur from slag on the hydration characteristics of slag cement, except for the cement-slag system, one model system only containing $C_3S$ and slag was studied. $C_3S$, the main constituent of cement, was mixed with slag to simplify the chemical composition of mixture and reduce the interference from other components. No other source of sulfur, such as sulfate originated from gypsum, was introduced into the system except for the existence of sulfur rich species in slag. The slag to cement (or $C_3S$) mass ratio was 7/3 and water to binder ratio was 0.4 (Table 2). Cement-quartz paste was also cast as a reference.

TAM Air isothermal calorimeter was employed to observe heat evolution of the paste samples at 20 °C for 7 days. Mixtures were mixed at a high speed for 2 min, and approximately 7 g of the binder was transported to a glass ampoule, sealed and placed in the calorimeter. The specimens were prepared in the same manner and mounted in a plastic bottle of 20 mL, which was sealed with thin Para film to avoid any evaporation. Sealed curing was performed for all specimens at 20 ± 3 °C until 3 months.

The compressive strength test was measured on slag cement paste cube (20 × 20 × 20 mm) prepared with the same recipe mentioned above after 1, 3, 7 and 28 days of sealed curing at 20 ± 3 °C in the laboratory. 5 paste cubes were performed at each testing age, using a procedure similar to EN 196-1.

Before X-ray diffraction (XRD) measurement and thermogravimetric analysis (TGA), the hydration of specimen was stopped by solvent exchange using isopropanol (For samples after 7 days curing, the isopropanol solution was refreshed frequently.). Slices cut from the specimens were crushed and ground to below 63 μm. X-ray powder diffraction was performed on a Philips PW 1830/40 Powder

**Table 1**
Chemical compositions (wt.%) determined by XRF analysis and physical properties of cement and slags.

| | Cement | CS1 | CS2 | SS |
|---|---|---|---|---|
| CaO | 64 | 37.40 | 37.97 | 37.04 |
| $SiO_2$ | 20 | 37.82 | 35.60 | 37.79 |
| $Al_2O_3$ | 5 | 13.58 | 13.12 | 14.51 |
| MgO | – | 8.11 | 7.24 | 8.83 |
| $FeO/Fe_2O_3$ | 3 | 0.36 | 0.37 | 0.28 |
| $TiO_2$ | – | 1.22 | 1.00 | 0.70 |
| $MnO/Mn_2O_3$ | – | 0.30 | 0.35 | 0.17 |
| $Na_2O_{eq}$[a] | 0.58 | 0.53 | 0.74 | 0.40 |
| $SO_3$ | 2.93 | 0.93 | 0.99 | 0.01 |
| LOI[b] | 1.20 | −0.87 | −1.27 | −0.02 |
| Physical properties | | | | |
| $d_{50}$ (μm)[c] | 26.81 | 20.94 | 16.90 | 22.73 |
| SSA ($m^2/g$)[d] | 0.284 | 0.937 | 1.162 | 0.895 |

[a] The $Na_2O_{eq}$ used here for cement and slag was identical, namely $Na_2O + 0.658 \times K_2O$.
[b] The loss-on-ignition (LOI) of CEM I 42,5N was provided by ENCI, while for slag, it was determined by thermogravimetric analysis at 950 ± 50 °C. The negative value of LOI is related to the oxidation of sulfur rich species in slag. It should be noted that the LOI value was not corrected in the XRF measurement.
[c] The particle size distribution (PSD) of slag was measured by EyeTech, Ankersmid. The $d_{50}$ of quartz is 24.21 μm.
[d] The specific surface area (SSA) of cement and slag was measured by Blaine and nitrogen adsorption with the BET method respectively.

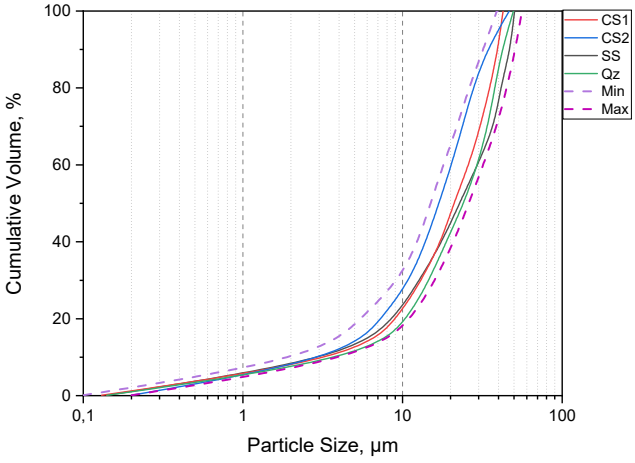


**Fig. 1.** Particle size distribution of slag and quartz. It is apparent that curves are limited in a narrow range, and slag CS2 is a little finer than others, which is also indicated by its $d_{50}$.

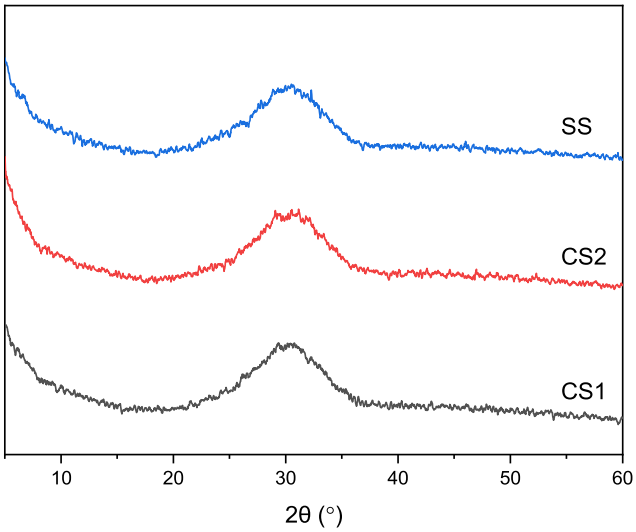


**Fig. 2.** XRD scan of three slags used in the present research.

**Table 2**
Mixtures of specimen (g).

| | Cement | $C_3S$ | Slag | Water | w/b |
|---|---|---|---|---|---|
| Cement-slag | 30 | - | 70 | 40 | 0.4 |
| $C_3S$-slag | - | 30 | 70 | 40 | 0.4 |

diffractometer employing the Cu K-alpha radiation. The machine was operated with an acceleration voltage of 40 kV and an X-ray beam current of 40 mA. Analysis was performed with a step size of 0.03° for a 2θ range from 5° to 60°. Thermogravimetric analysis was performed on Netzsch STA 449 F3 Jupiter under Argon atmosphere. About 40 mg of the specimen powder was heated from 40 to 900 °C with a heating rate of 10 °C/min in an $Al_2O_3$ crucible with an identical crucible as reference.

Mercury intrusion porosimetry (MIP) measurement was also carried out to measure pore size distribution. Samples were crushed into small slices, immersed into isopropanol solution to stop hydration, and stored on vacuum to constant weight subsequently. The maximum pressure applied by the instrument was 210 MPa, and each measurement process contains three steps: intrusion of mercury at low pressure from 0 to 0.170 MPa; intrusion at high pressure from 0.170 to 210 MPa and extrusion of mercury back to 0.170 MPa. The relationship between pore radius and pore pressure was elaborated in Washburn equation, of which the surface tension of mercury is 0.485 N/m at 25 °C and the contact angle between mercury and specimen was 140°.

To acquire backscattered electron (BSE) micrographs of the selected samples, slices of hydrated paste specimens were sawn and immersed in isopropanol solution for hydration stop, dried at 40 °C, impregnated with epoxy resin and polished with diamond paste down to 0.25 μm. They were further coated with carbon and examined using FEI QUANTA FEG 650 ESEM with an accelerating voltage of 15 kV and a working distance of 10 mm. X-ray energy dispersive (EDS) detector was used to determine the elemental composition of hydration products. Approximately 150 points per sample were analyzed.

## 3. Result and discussion

### 3.1. The color of hydrated powder

The hydrated powders of cement-slag CS1 and CS2 blends display a dark green coloration ("greening effect") as Fig. 3 displays. This is known to originate from the formation of blue-green metal sulfides such as CaS, FeS, MnS etc. during hydration and oxidation under anoxic conditions [16], or charge transfer processes in various phases or complexes, such as green rust [17]. The existence of sulfur species incorporated in slag CS1 and CS2 was also confirmed from the negative LOI value. As for cement-slag SS blend, it shows white coloration as there was negligible sulfur content available in the model paste.

### 3.2. Compressive strength

Compressive strength values of slag cement paste cubes at 1, 3, 7 and 28 days are reported in Table 3 respectively. Although from different origins and presenting a little difference in particle size distribution, commercial slag CS1 and CS2 show almost identical compressive strength development. Synthetic slag SS performs comparably to commercial slag at 1 day, and from then on, a lower compressive strength is reached by it compared with that of commercial slag.

### 3.3. Kinetics of hydration

#### 3.3.1. Heat of hydration

Fig. 4 shows the heat evolution rate (a) and cumulative heat release (b) for all blends, normalized to per gram of cement. The cement-quartz blend was dominated by one main peak, associated with the hydration of alite in cement, followed by a shoulder after 1 day, indicative of the secondary aluminate reaction upon sulfate depletion [18,19]. The hydration of cement-slag blends were quite similar except for the enhanced secondary aluminate reaction. During dormant period, the intensities of cement-slag blends were higher than that of cement-quartz mixture, however, the curves were almost identical with each other after entering

**Table 3**
Results of compressive strength test on slag cement paste cube with 95% confidence intervals calculated from 5 replicates (MPa).

| | 1d | 3d | 7d | 21d | 28d |
|---|---|---|---|---|---|
| CS1 | 3.2±0.2 | 13.1±0.9 | 22.6±1.3 | 30.4±1.6 | 48.5±2.0 |
| CS2 | 3.2±0.2 | 13.2±1.1 | 23.2±1.5 | 31.2±1.5 | 50.0±1.8 |
| SS | 3.1±0.3 | 10.5±0.8 | 19.1±0.9 | 26.8±1.6 | 43.3±2.1 |

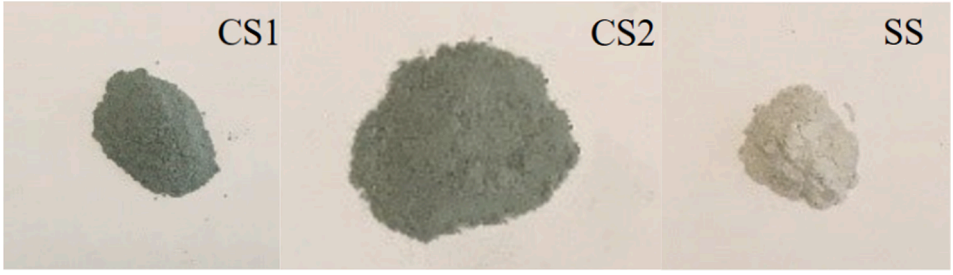


**Fig. 3.** The coloration of hydrate power from different cement-slag blends. The green coloration is attributed to a complex reaction of sulfur species in slag with other components of cement. (For interpretation of the references to color in this figure legend, the reader is referred to the web version of this article.) (For interpretation of the references to color in this figure legend, the reader is referred to the web version of this article.)

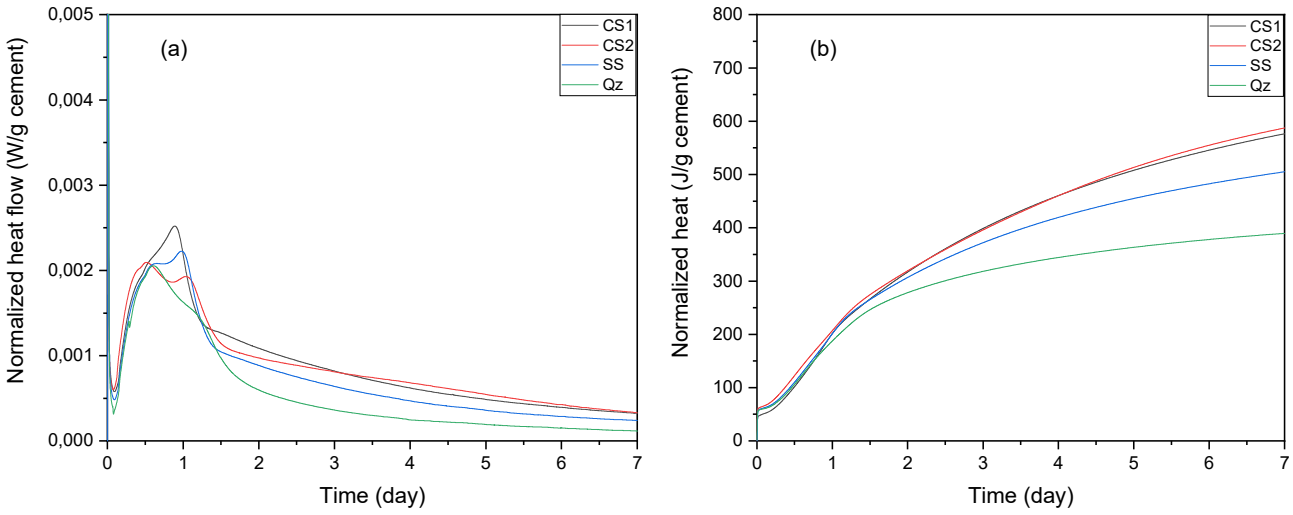


**Fig. 4.** Calorimetric curves of cement-slag and quartz system. (a) normalized heat flow; (b) normalized heat release.

acceleration period, meaning that slag could be regarded as inert filler like quartz during this age. It is also confirmed by compressive strength development as shown in Table 3, which is about 3.0 MPa after 1 day both for commercial and synthetic slag. Slag CS2 presents a little faster hydration rate during nucleation and growth stage due to its finer particle size.

After the main hydration peak, the second aluminate reaction peak in cement-slag blend occurs earlier and seems to be more intense compared with that in cement-quartz blend (Fig. 4 (a)). On one hand, this could be the consequence of physical replacement while on the other hand, the possibility of a small amount of reaction cannot be excluded between the slag grains and increased calcium hydroxide content produced by the hydration of cement, considering this high level of slag replacement [20,21].

The hump after the second aluminate reaction peak could be distinguished from mixtures containing slag and quartz. This peak corresponds to the pozzolanic reaction between slag and $Ca(OH)_2$, liberated from the hydration of cement, when a sufficient amount of $Ca(OH)_2$ and alkalinity was reached. Moreover, continuous transformation of ettringite (AFt) to calcium monosulfoaluminate (Ms) was also included in this hump in all blends.

The curves of total heat release deviate from each other after 1 day (Fig. 4 (b)), indicating that slag starts to participate in the pozzolanic reaction from there on. Although there is a slight difference of chemical composition and fineness between commercial slag CS1 and CS2, the heat evolution was almost the same at 7 days, which implies that the same amount of reaction occured concerning these two blends. The compressive strength values of these two commercial slags are almost same at 7 days at about 30.0 MPa. It is also worthwhile to note that while slag CS1 and SS had comparable chemical composition and fineness, a significant difference in the total heat release (~70 J/g) at 7 days was found between them, leading to a ~5.0 MPa less compressive strength reached by synthetic slag SS. Actually, it is the sulfur content of slag that dominates the difference in total heat release after one day, and it will be discussed in Part 3.5.

### 3.3.2. Bound water and portlandite

Bound water (BW) is assumed to be the water chemically fixed in the hydrated phases and often referred to as non-evaporable water. Commonly it is bound in hydrates in the form of e.g. C–S(A)–H, AFt, AFm-phase (mainly Ms), hydrotalcite-like phase (Ht), portlandite. It accounts for most of the water in C–S(A)–H gel, which is of particular interest owing to its contribution to strength development. The bound water content is an index of hydration degree to some extent, however, it cannot be taken as the overall degree of hydration directly as different hydrates contain different amounts of water which can be decomposed at different temperatures, especially for blended cement. When there is an overlap in the decomposition temperature of hydrates, it is difficult to distinguish from which hydrate the water comes from.

The bound water content as calculated from a TGA graph and corrected for the water bound in portlandite is present in Fig. 5 (a) according to the following formula:

$$BW = \left(\frac{W_{50} - W_{550} - W_{H_2OCH}}{W_{550}}\right) \times 100\%$$

with $W_{50}$ = sample weight at 50 °C, $W_{550}$ = sample weight at 550 °C and $W_{H_2OCH}$ = mass loss from dehydroxylation of portlandite by tangent method. It is found that the bound water content of all these blends show an increasing trend with time, and the amount among CS1, CS2 and SS is comparable up to 3 months, of which cement-slag CS2 binds the most water.

Fig. 5 (b) depicts the amount of portlandite produced in blend with time. It is estimated based on the weight loss between 400 °C and 500 °C from TGA due to the dehydroxylation of $Ca(OH)_2$ through tangent method. The portlandite content remained in cement-slag blend could also be regarded as an index of hydration degree, indicating the extent of pozzolanic reaction between slag and $Ca(OH)_2$. The portlandite content in cement-slag blend decreases from 7 days to 3 months, suggesting the progress of pozzolanic reaction. Actually, the difference of portlandite content among three slags was too small to differentiate them. Conversely, the amount of portlandite increases until 3 months in cement-quartz blend without consumption by slag. Taking cement-quartz as a reference, it was calculated that about half of the portlandite liberated from cement hydration was consumed by the pozzolanic activity after 7 days and about two-thirds after 3 months, of which slag CS1 consumes the most portlandite.

## 3.4. Hydration products

TGA result of the cement-slag system is shown in Fig. 6. The main hydrates formed in these blends were the same, and the cumulative mass loss of the CS samples was comparable to each other. The mass loss between 400 and 500 °C arose from the dehydroxylation of portlandite. Although the peaks for AFt and C–S(A)–H were overlapped at 100–150 °C, their precise deconvolution was possible. The shoulder at ~200 °C and the hump at ~300 °C implied the presence of Ms. Ht could also be detected with a distinct peak located at approximately 350 °C.

X-ray diffractograms in Fig. 7 reveal the presence of portlandite and

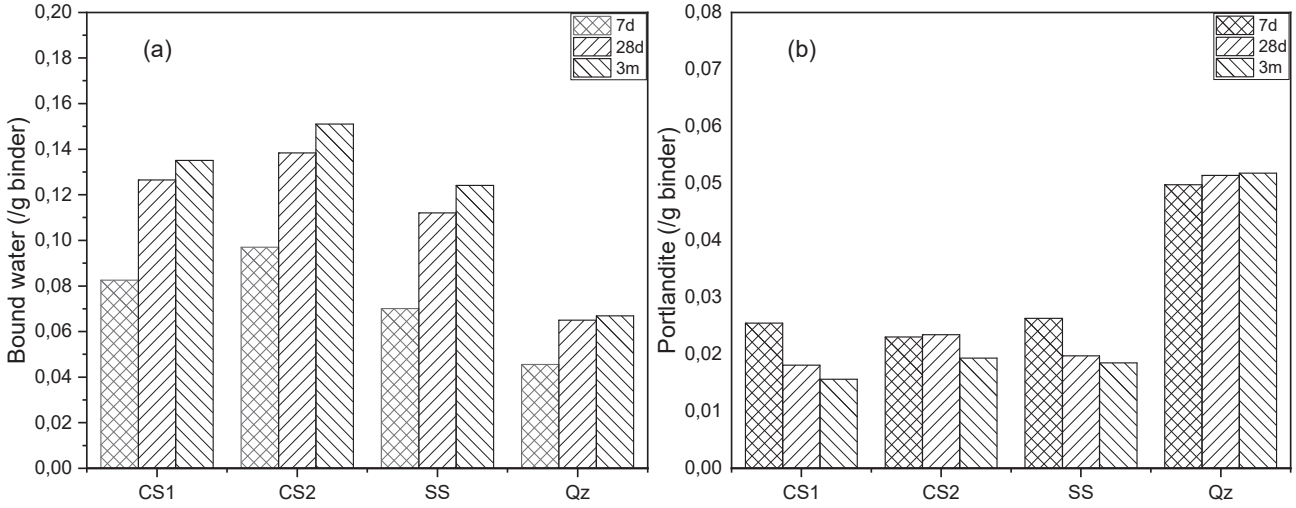


**Fig. 5.** (a) Bound water and (b) Portlandite contents of cement-slag and quartz system.

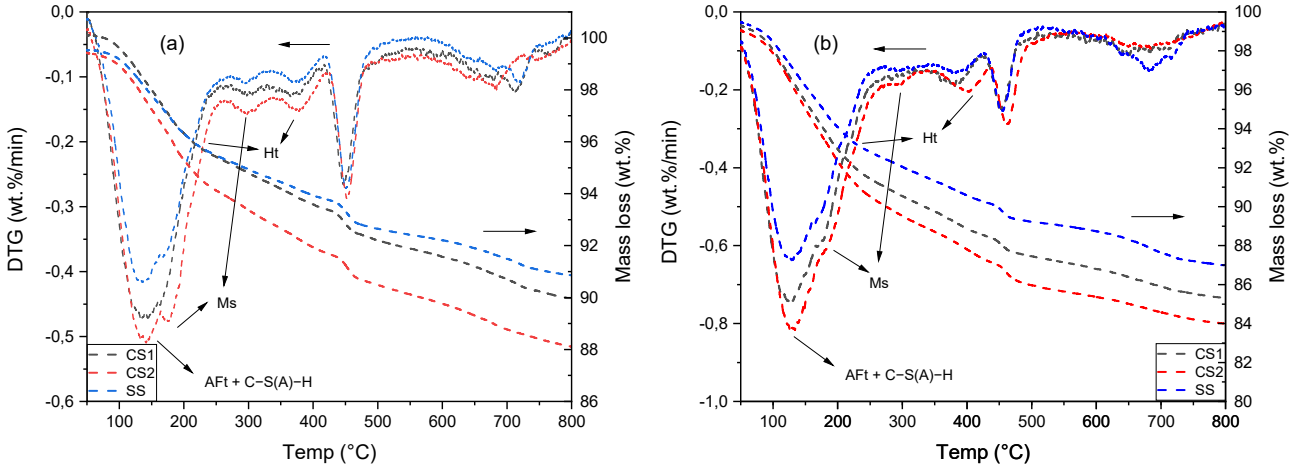


**Fig. 6.** TGA result of cement-slag system after curing of (a) 7 days and (b) 3 months.

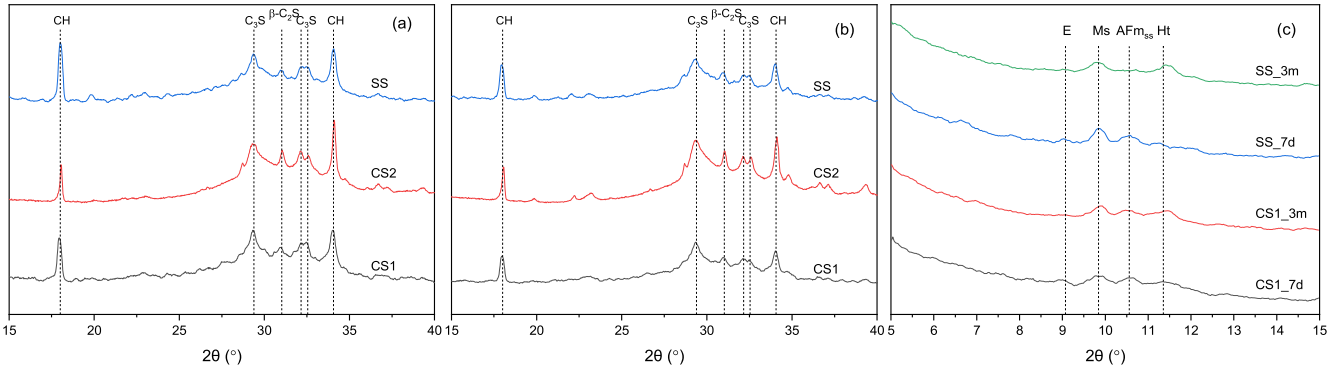


**Fig. 7.** Typical results of XRD analysis of cement-slag system after curing of (a) 7 days and (b) 3 months; (c) XRD patterns from 5 to 15° (2θ) highlight the presence of AFm-phases. E: ettringite; AFm$_{ss}$: solid solution of hemicarbonate and $OH^-$ substituted monosulfate.

unhydrated $C_3S$ and $C_2S$ in the cement-slag mixtures at specific ages. For C–S(A)–H, the main peaks were located at around (2θ = ) 30°, which was very difficult to distinguish from that of $C_3S$. As shown in Fig. 7 (a) and (b), the peak intensity of portlandite decreases from 7 days to 3 months as a result of pozzolanic activity. The transformation from AFt to Ms proceeds continuously with hydration, and Ms starts to dominate as early as from 7 days on (Fig. 7 (c)). The peak for Ht was more visible while it becomes negligible for AFt after 3 months. It should also be noted that there is AFm solid solution (AFm$_{ss}$) of hemicarbonate and $OH^-$ substituted monosulfate as detected by XRD [22], and it is more likely to be AFm-OH phase. For one thing, there was no carbonate phase involved in the system, and for another, the peak intensity of AFm$_{ss}$ varied consistently with portlandite content in the system with time.

### 3.5. Microstructure

#### 3.5.1. Pore structure of the paste samples

Findings of mercury intrusion porosimetry (MIP) on the paste samples after 7 days and 3 months of curing are shown in Fig. 8. Results show that the hydration products of the pozzolanic reaction between calcium hydroxide and slag further refined and densifed the pore structure, which is illustrated in Fig. 8 (a) and (b). At 7 days, mixtures of commercial slag CS1 and CS2 presented a relatively finer critical pore diameter than that of synthetic slag SS, however, the pore size distribution and total porosity for these three cement-slag blends were almost identical, irrespective of the origin and fineness after 3 months of curing.

#### 3.5.2. Sem-BSE

Fig. 9 shows typical BSE micrographs of cement-slag CS1 and cement-SS blends after 3 months of curing. A close mixture of unhydrated cement and slag grains, hydrated phases and pores were observed as the main phases forming the microstructure. Unhydrated cement grains (e.g. circle 1) were observed even after 3 months. Only a few AFt clusters were observed, while monosulfate exists as widespread, fine and compact clusters intermixed with C–S(A)–H (circled and labelled 2) [23]. Hydration rim in the slag particles indicated slow hydration even after 3 months. On the other hand, after 3 months of curing, hydrated phases were observed as precipitates circumscribing the unhydrated slag particles.

#### 3.5.3. Chemical composition of matrix

Hydration products in the matrix and the hydration rims of unhydrated cement and slag particles were characterized by SEM-EDS microanalysis with internal standard (standardless microanalysis). It is worthwhile to mention that the accelerating voltage used for matrix analysis is 15 kV under high vacuum condition, and to eliminate the interference from matrix nearby, 8 kV is employed for slag rim analysis. The determined atomic ratios of Al/Ca against Si/Ca are presented in Fig. 10 showing the change in chemical composition of C–S(A)–H phase as a function of time. Additionally, the Ca/Si and Al/Si ratios were calculated and summarized in Table 4, similar to the works of [24–25].

The Ca/Si atomic ratio in all blends remains to be constant over time with a value fluctuating at around 1.25 while the change of Al/Si atomic ratio appears to be complicated. In the case of SS blend, the Al/Si atomic ratio was shown to be approximately unchanged irrespective of curing time, with a value close to 0.10. However, in slag CS1 and CS2 blends, the Al/Si ratio was higher especially at 7 days, and it decreases slightly after 3 months of curing. The higher Al/Si ratio seems to be related to the extra sulfur content in commercial slag blends, the release of which accompanied by the dissolution of slag attracts more aluminum into matrix at early age. All in all, the Ca/Si and Al/Si ratios measured in these mixtures were consistent with those found in [26–28], where the massive incorporation of slag into cement leads to C–S(A)–H with a lower Ca/Si and higher Al/Si atomic ratio was ultimately formed.

The atomic ratio of S/Ca versus Al/Ca in cement-slag CS1 and SS mixtures shown in Fig. 11 illustrates that the hydrated assemblages of the matrix at investigated age was dominated by C–S(A)–H and Ms. At 7 days, the S/Ca ratio of the matrix of CS1 was higher than that of SS, whereas the difference between them becomes negligible at 3 months. The higher S/Ca ratio after 7 days in CS1 highlights the contribution from sulfur in commercial slag. It is also confirmed by the calorimetric measurement (Fig. 4 (b)) where more heat was released by the CS1 and CS2 blends after 1 day and the difference was apparent until 7 days. Moreover, it should be noted that higher Al/Si ratio observed in CS1 and CS2 matrices at 7 days (Fig. 10 (a) and Table 4 was also associated with the liberation of sulfur from slag, which promoted the release of aluminum from slag into matrix.

#### 3.5.4. Chemical composition of slag hydration rim

Hydrotalcite-like phase is the main precipitation from the hydration of slag, where the Mg/Al ratio is close to 2 [27,29]. Mg/Al atomic ratio was obtained from the slope of the line of best fitting when plotting Mg/Si against Al/Si. Fig. 12 (a) shows that the rim around unhydrated slag particle in cement-slag SS blend is very apparent after 3 months. It is noted that the Mg/Al ratio of the slag rim is a little higher in cement-slag CS1 blend of 2.12 than that in cement-slag SS blend of 1.56. Here it is worthwhile to mention that 8 kV was employed for point analysis in slag rim. In fact, the rim of slag is not thick enough after 3 months of curing to get rid of interference from the unhydrated slag particle and the surrounding matrix totally. If a higher accelerated voltage is used, the interaction volume will be larger, and there is certainly more contaminations from the surrounding in the results. Moreover, one needs to keep in mind that hydrotalcite-like phase is distributed unevenly in the rim, similar to the Liesegang phenomenon of rhythmic precipitation when containing two or more diffusion species which can react together after reaching a critical supersaturation [30–32].

### 3.6. The effect of sulfur in slag

European Standard EN 15167-1 requires that the sulfide and sulfate contents in slag should be $\leq$2.0% and 2.5% respectively. The main concern is the delayed formation of ettringite when exceeding this certain amount. Also, doubts were being expressed that whether the sulfide content of slag would promote reinforcement corrosion. Thus, to understand the effect of sulfur from slag on the hydration evolution specifically, model $C_3S$-slag CS1 and SS systems were employed. $C_3S$, the

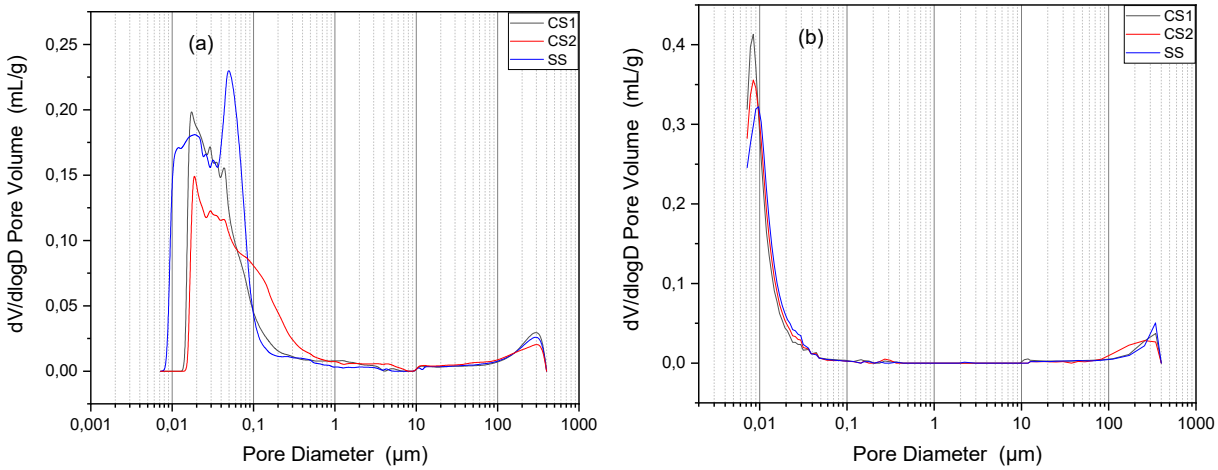


**Fig. 8.** Differential pore size distribution of samples measured after (a) 7 days and (b) 3 months.

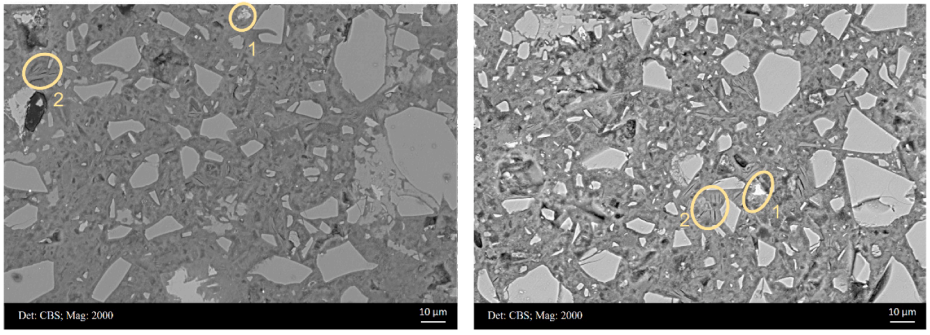


(a) (b)

**Fig. 9.** Microstructure of cement-slag (a) CS1 and (b) SS paste after 3 months of mixing. 1: Unhydrated cement grain; 2: fine and compact crystal of monosulfate.

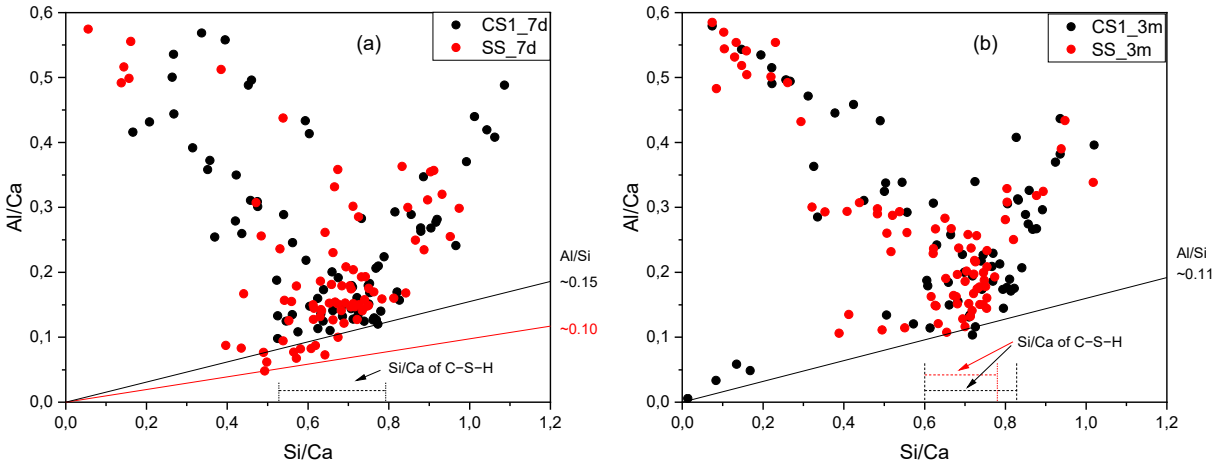


**Fig. 10.** Atomic ratio of Al/Ca against Si/Ca of cement-slag system after (a) 7 days and (b) 3 months of curing.

**Table 4**
Changes in Ca/Si and Al/Si ratios of C–S(A)–H phase, and Mg/Al of hydrotalcite phase.

| | | 7 days | 3 months |
|---|---|---|---|
| CS1 | Ca/Si | ~1.25 | ~1.21 |
| | Al/Si | ~0.15 | ~0.11 |
| | Mg/Al | – | ~2.12 |
| CS2 | Ca/Si | ~1.19 | ~1.23 |
| | Al/Si | ~0.17 | ~0.16 |
| | Mg/Al | – | ~2.08 |
| SS | Ca/Si | ~1.25 | ~1.28 |
| | Al/Si | ~0.10 | ~0.11 |
| | Mg/Al | – | ~1.56 |

main constituent of cement, was mixed with slag to simplify the chemical composition of mixture and reduce the interference from other components. No other source of sulfur, such as sulfate originated from gypsum, was introduced into the system except for the existence of sulfur rich species in slag.

### 3.6.1. Heat of hydration

As shown in Fig. 13, it was found that the sulfur incorporated in slag plays a key role on the hydration of $C_3S$-slag blend. On the one hand, the dormant period ends a little earlier in $C_3S$-CS1 blend paste (Fig. 13 (a)). It is well recognized that $Al^{3+}$ ions have a perturbing effect on the reactivity of silicates [33–37] depending mainly on the concentration of aluminate and pH of the solution [35–37]. $Al^{3+}$ ion adsorbed on the reactive site of $C_3S$ seems to be removed by $SO^{4-}$ ion sourcing from sulfur incorporated in slag CS1 immediately, thus shortening the induction period. On the other hand, there is a small decrease of the intensity of main hydration peak for the $C_3S$-SS blend. Moreover, a hump (labelled A) occurs in $C_3S$-slag CS1 blend after 1 day (Fig. 13 (a)), indicative of secondary reaction between $Al^{3+}$ ion and $SO^{4-}$ ion sourcing from sulfur incorporated in slag CS1. It was also confirmed by the total heat release shown in Fig. 13 (b), ~50 J/(g $C_3S$) more heat was released by the $C_3S$-CS1 blend than that of the $C_3S$-SS blend.

### 3.6.2. Hydration products

XRD scan focused on 8–13° (2θ) reveals the presence of Ht in the $C_3S$-CS1 and the $C_3S$-SS blends (Fig. 14, whose peak was increasingly visible with time. A distinct peak between 10 and 11° occurs in the mixture of $C_3S$-CS1 after 3 months of curing. As mentioned earlier, it implies the existence of AFm solid solution ($AFm_{ss}$) of hemicarbonate and $OH^-$ substituted monosulfate. It also demonstrates that the sulfur contained in the CS1 grains participates in the formation of AFm-$SO_4$ phase eventually. The amount of sulfur released by slag was very small at the beginning, proved by the low hump in the calorimetric measurements and no apparent peak in XRD pattern after 7 days in $C_3S$-CS1 blend. Hemicarbonate originates probably due to the carbonation of AFm-$SO_4$ phases during sample preparation. Furthermore, there was no peak indicating the presence of an AFm-phase in the hydrated $C_3S$-SS system.

The atomic ratio of S/Ca against Al/Ca of the matrix in $C_3S$-CS1 blend was shown in Fig. 15 (The atomic ratio of S/Ca against Al/Ca of the matrix in $C_3S$-slag SS blend is not shown here as S/Ca ratio of it equals to 0 approximately.). It illustrates that the hydrated assemblages of the matrix at investigated ages were dominated by C–S–H and Ms. The S/Ca ratio of matrix in slag CS1 blend after 3 months of curing was

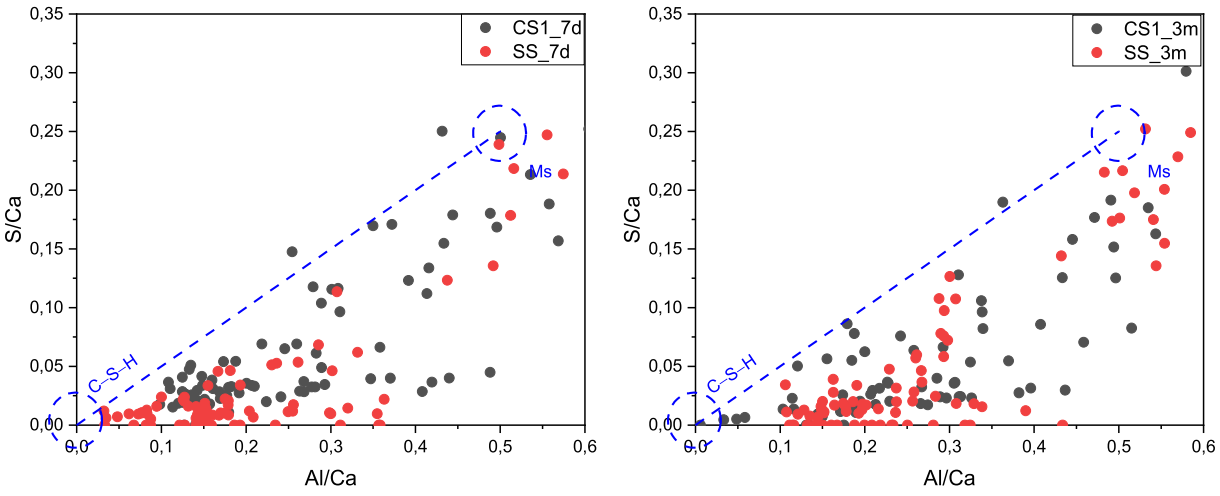


**Fig. 11.** Atomic ratio of S/Ca against Al/Ca of cement-slag system after (a) 7 days and (b) 3 months of curing.

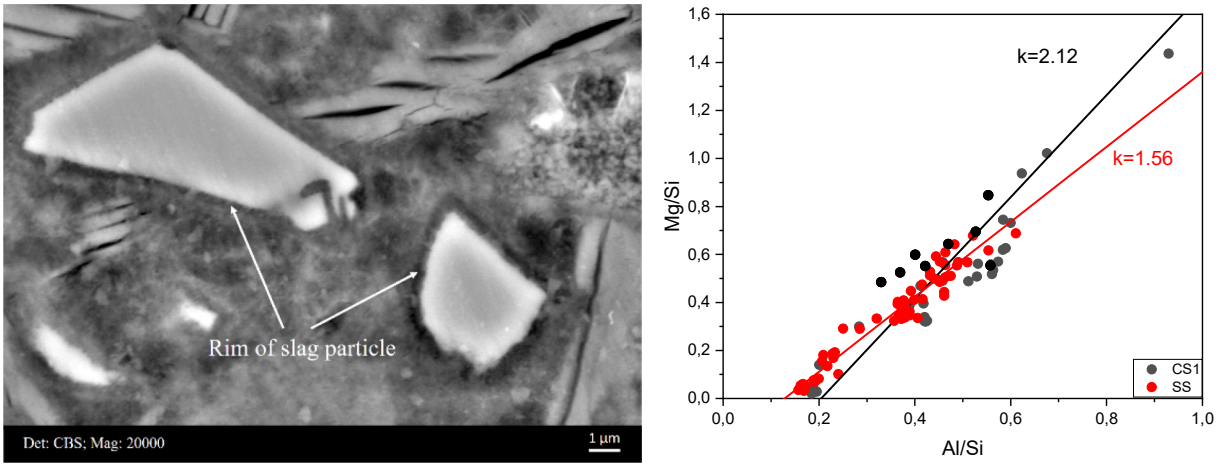


**Fig. 12.** (a) A typical hydration rim of an unhydrated slag particle from cement-slag SS blend; and (b) Atomic ratio of Mg/Si against Al/Si of cement-slag system after 3 months of curing.

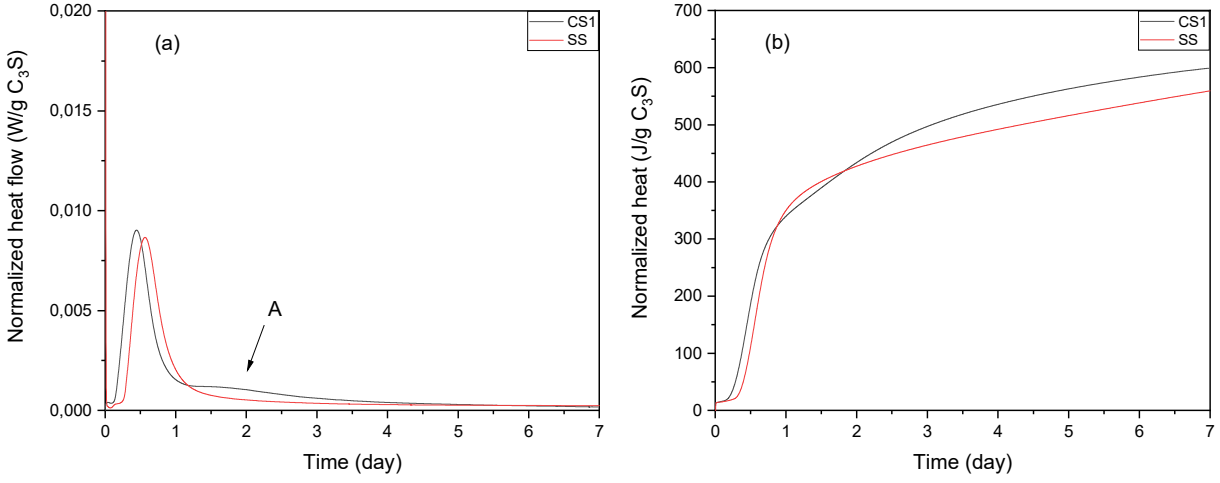


**Fig. 13.** (a) Heat flow and (b) total heat release as a function of time in calorimetric measurement for $C_3S$-slag CS1 and SS system.

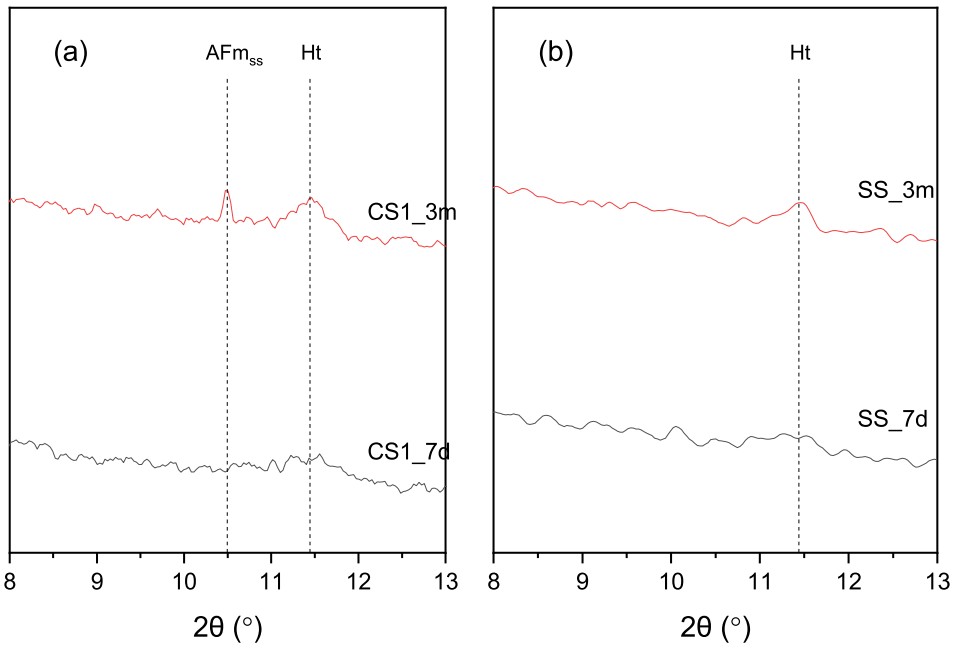


**Fig. 14.** XRD patterns from 8 to 13° (2θ) of (a) $C_3S$-slag CS1 and (b) $C_3S$-slag SS blends highlight the presence of Ht and AFm-phase. Ht: hydrotalcite; $AFm_{ss}$: solid solution of hemicarbonate and $OH^-$ substituted monosulfate.

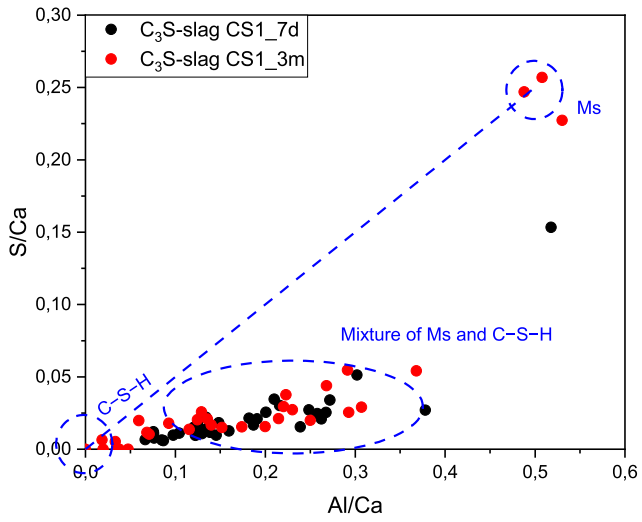


**Fig. 15.** The atomic ratio of S/Ca against Al/Ca of the matrix in $C_3S$-slag CS1 blend after 7 days and 3 months of curing.

slightly higher than that after 7 days, suggesting more sulfur was released by slag CS1 and it was involved in the formation of hydrates in the matrix.

## 4. Thermodynamic modelling

Thermodynamic modelling was also carried out to investigate the effect of sulfur content of slag on the hydration characteristics using the Gibbs free energy minimization software GEMS [38–39] with thermodynamic data from the PSI-GEMS [40–41] supplemented by cement specific data [42–43]. The calcium-alkali aluminosilicate hydrate ideal solid solution model (CNASH_ss) proposed by Myers et al. [44] was employed to describe the C–(N–)A–S–H gel in the studied systems, which was able to account for the incorporation of elements other than Ca, Si, H and O into the structure of C–S–H gel. MA-OH-LDH_ss containing three end-members with Mg/Al ratios of 2, 3 and 4 reformulated into an ideal solid solution [45] was employed to perform the modelling of hydrotalcite-like solid solution series. The mixing proportion and chemical composition of CEM I and CS1 as reported in Table 1 were used as input data. For simplicity, some assumptions were introduced. For example, reactants of different degrees of hydration were assumed, and it was postulated that slag dissolves congruently.

The reaction degree of clinker phases of cement as a function of time was estimated using the empirical kinetic approach of Parrot and Killoh [46], and the parameters were given elsewhere in [47]. Logistic function was selected and used to fit the 7 days normalized heat difference between cement-slag and cement-quartz blends, and extrapolated until 3 months to calculate the hydration degree of slag.

Thermodynamic modelling of the hydrate assemblages as a function of sulfur content incorporated in CS1 in cement-slag systems is displayed Fig. 16. It is found that more Ms will form with the gradual increase of sulfur content in slag with the consumption of strätlingite and

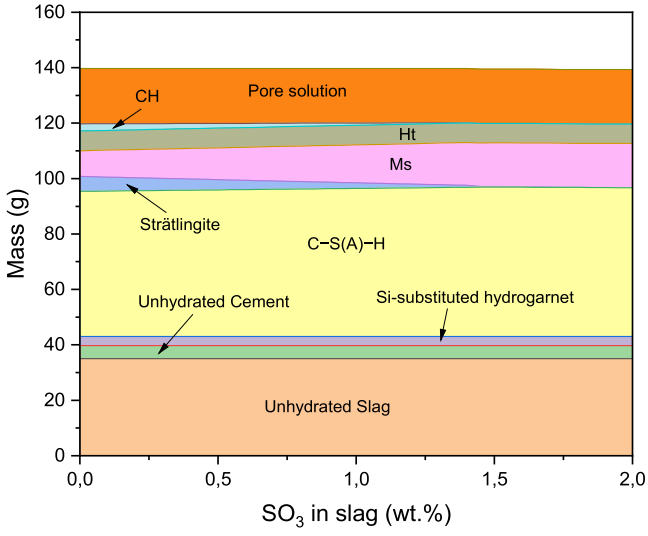


**Fig. 16.** Hydration products of (a) cement and (b) $C_3S$-slag systems according to the thermodynamic modelling after 3 months of curing.

portlandite according to the following equation 1. It is consistent with experiment results shown in Fig. 5, compared with cement-slag SS mixture, less portlandite and more bound water was observed in cement-slag CS1 blend, which could be ascribed to the addition of sulfur species in slag CS1. The $SiO_3^{2-}$ ion produced was adsorbed and responsible for the very small increase in the mass of C–S(A)–H. Moreover, the amounts of Ht and pore solution in the binder seem to be unaffected by the variation of sulfur content of slag.

$$Ca_2Al_2SiO_2(OH)_{10}\cdot 3H_2O + 2Ca(OH)_2 + SO_4^{2-} + 2H_2O \rightarrow Ca_4Al_2(SO_4)(OH)_{12}\cdot 6H_2O + SiO_3^{2-} \quad (1)$$

In the model, the absorption of $SO_4^{2-}$ by C–S(A)–H was not taken into consideration. It was found through the modelling that all sulfur released from slag contribute to the formation of Ms. Unlike aluminum which is incorporated in the compound structure of the C–S–H, zeta potential experiment on C–S–H demonstrated that sulfate is adsorbed on the surface of C–S–H, and could easily be desorbed when the sulfate concentration in pore solution drops [48].

## 5. Conclusions

The paper evaluates the reliability of synthetic slag produced in the laboratory used to simulate the granulated blast furnace slag employed in the cement industry and specifies the role of sulfur in slag on the hydration process. The findings of this study lead to the following conclusions:

- The origin of slag has very few impact on the hydration process of cement-slag system when parameters such as chemical composition and amorphous content are kept the same.
- Regarding the compressive strength development of slag cement paste, synthetic slag SS performs comparably to commercial slag at 1 day, and from then on, a lower compressive strength is reached by it compared with that of commercial slag until 28 days.
- The sulfur in slag starts to participate in hydration already after one day and it dominates the difference of heat release according to the calorimetric measurements, consistent with the result of compressive strength test. Sulfur affects the pore structure and element composition of the matrix at 7 days significantly, and higher Al/Si and S/Ca ratios detected in cement-CS1 and cement-CS2 blends can be attributed to the activity of sulfur in slag. However, the effect becomes negligible at 3 months.
- The simulation results of the $C_3S$-slag model paste confirms participation of sulfur in the hydration reactions after 1 day and involves into the formation of AFm-$SO_4$ phase eventually.
- Thermodynamic modelling shows that more Ms will precipitate with the gradual increase of sulfur content in slag at the expense of strätlingite and portlandite consumption. The amounts of Ht and pore solution in the binder are unaffected by the variation of sulfur content of slag.

*CRediT authorship contribution statement*

**Yu Zhang:** Investigation, Methodology, Writing – original draft, Writing – review & editing. **Erik Schlangen:** Supervision, Writing – review & editing. **Oğuzhan Çopuroğlu:** Supervision, Funding acquisition, Writing – review & editing.

## Declaration of Competing Interest

The authors declare that they have no known competing financial interests or personal relationships that could have appeared to influence the work reported in this paper.

## Acknowledgements

China Scholarship Council (the Grant Number 201808320456) and BAM Infraconsult B.V. are gratefully acknowledged for their financial support. Authors thank Arjan Thijssen and Maiko van Leeuwen (Microlab, TU Delft) for their technical support. René Albers (Ecocem Benelux BV) is gratefully acknowledged for providing commercial slag samples.

## References

[1] Juenger, M., et al., *Advances in alternative cementitious binders.* 2011. **41**(12): p. 1232–1243.
[2] Crossin, E.J.J.o.C.P., The greenhouse gas implications of using ground granulated blast furnace slag as a cement substitute. 2015. **95**: p. 101-108.
[3] Li, Y., et al., Environmental impact analysis of blast furnace slag applied to ordinary Portland cement production. 2016. **120**: p. 221–230.
[4] J. Bijen, Benefits of slag and fly ash, Constr. Build. Mater. 10 (5) (1996) 309–314.
[5] Sohn, I., D.J.J.s.r.i. Min, A review of the relationship between viscosity and the structure of calcium-silicate-based slags in ironmaking. 2012. **83**(7): p. 611–630.
[6] Özbay, E., et al., Utilization and efficiency of ground granulated blast furnace slag on concrete properties–A review. 2016. **105**: p. 423-434.
[7] Sajid, M., et al., Understanding the structure and structural effects on the properties of blast furnace slag (BFS). 2019. **59**(7): p. 1153-1166.
[8] P.T. Durdziński, R. Snellings, C.F. Dunant, M.B. Haha, K.L. Scrivener, Fly ash as an assemblage of model Ca–Mg–Na-aluminosilicate glasses, Cem. Concr. Res. 78 (2015) 263–272.
[9] A. Schöler, F. Winnefeld, M.B. Haha, B. Lothenbach, The effect of glass composition on the reactivity of synthetic glasses, J. Am. Ceram. Soc. 100 (6) (2017) 2553–2567.
[10] S. Kucharczyk, M. Zajac, C. Stabler, R.M. Thomsen, M. Ben Haha, J. Skibsted, J. Deja, Structure and reactivity of synthetic CaO-Al2O3-SiO2 glasses, Cem. Concr. Res. 120 (2019) 77–91.
[11] V.-J.-T.-Z. Sevieri, Beton aus granulierter Hochofenschlacke nach 27jähriger Einwirkung von, Meerwasser. 58 (1934) 587–589.
[12] Glasser, F.P., et al., *Modification of cement pore fluid compositions by pozzolanic additives.* 1988. **18**(2): p. 165–178.
[13] Gruskovnjak, A., et al., *Hydration of alkali-activated slag: comparison with ordinary Portland cement.* 2006. **18**(3): p. 119-128.
[14] Lothenbach, B., et al., *Hydration of a low-alkali CEM III/B–SiO2 cement (LAC).* 2012. **42**(2): p. 410-423.
[15] Kleinjan, W.E., A. de Keizer, and A.J.J.W.R. Janssen, *Kinetics of the chemical oxidation of polysulfide anions in aqueous solution.* 2005. **39**(17): p. 4093-4100.
[16] Le Cornec, D., et al., *Greening effect in slag cement materials.* 2017. **84**: p. 93-98.
[17] Schwab, A., et al., Characteristics of blast furnace slag leachate produced under reduced and oxidized conditions. 2006. **41**(3): p. 381-395.
[18] Quennoz, A., K.L.J.C. Scrivener, and C. Research, *Interactions between alite and C3A-gypsum hydrations in model cements.* 2013. **44**: p. 46-54.
[19] F. Zunino, K. Scrivener, Factors influencing the sulfate balance in pure phase C3S/C3A systems, Cem. Concr. Res. 133 (2020) 106085.
[20] Gruyaert, E., et al., Study of the hydration of Portland cement blended with blast-furnace slag by calorimetry and thermogravimetry. 2010. **102**(3): p. 941–951.
[21] Berodier, E.M.J., *Impact of the supplementary cementitious materials on the kinetics and microstructural development of cement hydration.* 2015, EPFL.
[22] Schöler, A., et al., Hydration of quaternary Portland cement blends containing blast-furnace slag, siliceous fly ash and limestone powder. 2015. **55**: p. 374–382.
[23] Scrivener, K.L.J.C. and c. Composites, *Backscattered electron imaging of cementitious microstructures: understanding and quantification.* 2004. **26**(8): p. 935–945.
[24] Deschner, F., et al., *Hydration of Portland cement with high replacement by siliceous fly ash.* 2012. **42**(10): p. 1389-1400.
[25] Whittaker, M., et al., The impact of alumina availability on sulfate resistance of slag composite cements. 2016. **119**: p. 356-369.
[26] Richardson, I.J.C. and C. Research, Tobermorite/jennite-and tobermorite/calcium hydroxide-based models for the structure of CSH: applicability to hardened pastes of tricalcium silicate, β-dicalcium silicate, Portland cement, and blends of Portland cement with blast-furnace slag, metakaolin, or silica fume. 2004. **34**(9): p. 1733-1777.
[27] Taylor, R., et al., Composition and microstructure of 20-year-old ordinary Portland cement–ground granulated blast-furnace slag blends containing 0 to 100% slag. 2010. **40**(7): p. 971–983.
[28] Escalante-Garcia, J.-I., J.J.C. Sharp, and C. Composites, *The chemical composition and microstructure of hydration products in blended cements.* 2004. **26**(8): p. 967-976.
[29] Whittaker, M., et al., The role of the alumina content of slag, plus the presence of additional sulfate on the hydration and microstructure of Portland cement-slag blends. 2014. **66**: p. 91-101.
[30] Glasser, F.J.M.s.o.c., Chemical, mineralogical and Micro-structural Changes Occurring in Hydrated Slag-Cement Blends. 1991: p. 41-82.
[31] Rodger, S.A. and G.W.J.A.i.C.R. Groves, *The microstructure of tricalcium silicate/pulverized-fuel ash blended cement pastes.* 1988. **1**(2): p. 84-91.
[32] Li, B., et al., Spatial zonation of a hydrotalcite-like phase in the inner product of slag: New insights into the hydration mechanism. 2021. **145**: p. 106460.
[33] B. Bickmore, et al., The Effect of Adsorbed Al (OH) 4-on the Dissolution Rate of Quartz. Eleventh Annual VM Goldschmidt Conference, 2001.

[34] Chappex, T., K.L.J.J.o.t.A.C.S. Scrivener, The effect of aluminum in solution on the dissolution of amorphous silica and its relation to cementitious systems. 2013. **96** (2): p. 592-597.
[35] Nicoleau, L., et al., *Ion-specific effects influencing the dissolution of tricalcium silicate.* 2014. **59**: p. 118-138.
[36] Pardal, X., et al., *27Al and 29Si solid-state NMR characterization of calcium-aluminosilicate-hydrate.* 2012. **51**(3): p. 1827-1836.
[37] Suraneni, P., R.J.J.C. Flatt, and C. Research, Use of micro-reactors to obtain new insights into the factors influencing tricalcium silicate dissolution. 2015. **78**: p. 208-215.
[38] Wagner, T., et al., GEM-Selektor geochemical modeling package: TSolMod library and data interface for multicomponent phase models. 2012. **50**(5): p. 1173-1195.
[39] Kulik, D.A., et al., GEM-Selektor geochemical modeling package: revised algorithm and GEMS3K numerical kernel for coupled simulation codes. 2013. **17**(1): p. 1-24.
[40] Hummel, W., et al., *Nagra Technical Report NTB 02-16.* 2002.
[41] Hummel, W., et al., *Nagra/PSI chemical thermodynamic data base 01/01.* 2002. **90** (9-11): p. 805-813.
[42] Matschei, T., et al., Thermodynamic properties of Portland cement hydrates in the system CaO–Al2O3–SiO2–CaSO4–CaCO3–H2O. 2007. **37**(10): p. 1379-1410.
[43] Lothenbach, B., et al., Thermodynamic modelling of the effect of temperature on the hydration and porosity of Portland cement. 2008. **38**(1): p. 1-18.
[44] Myers, R.J., et al., A thermodynamic model for C-(N-) ASH gel: CNASH_ss. Derivation and validation. 2014. **66**: p. 27-47.
[45] Myers, R.J., et al., *Thermodynamic modelling of alkali-activated slag cements.* 2015. **61**: p. 233-247.
[46] L. Parrot, Prediction of cement hydration. Proceedings of the British Ceramic Society, 1984.
[47] Lothenbach, B., et al., *Influence of limestone on the hydration of Portland cements.* 2008. **38**(6): p. 848–860.
[48] Nachbaur, L., et al., Electrokinetic properties which control the coagulation of silicate cement suspensions during early age hydration. 1998. **202**(2): p. 261-268.